Full-potential KKR within the removed-sphere method: A practical and accurate solution to the Poisson equation

Zhenhua Ning,[1,*] A. V. Smirnov,[1] William A. Shelton, Jr.,[1,2] and Duane D. Johnson[1,3,†]
[1]*Division of Materials Science and Engineering, Ames National Laboratory, Ames, Iowa 50011, USA*
[2]*Department of Physics and Astronomy, Louisiana State University, Baton Rouge, Louisiana 70803, USA*
[3]*Department of Materials Science and Engineering, Iowa State University, Ames, Iowa 50011, USA*

(Received 18 August 2022; revised 10 November 2022; accepted 14 November 2022; published 12 December 2022)

An efficient and accurate generalization of the removed-sphere method (RSM) to solve the Poisson equation for total charge density in a solid with space-filling convex Voronoi polyhedra (VPs) and any symmetry is presented. The generalized RSM avoids the use of multipoles and VP shape functions for cellular integrals, which have associated ill-convergent large, double-internal L sums in spherical-harmonic expansions, so that fast convergence in single-L sums is reached. Our RSM adopts full Ewald formulation to work for all configurations or when symmetry breaking occurs, such as for atomic displacements or elastic constant calculations. The structure-dependent coefficients A_L that define RSM can be calculated once for a fixed structure and speed up the whole self-consistent-field procedure. The accuracy and rapid convergence properties are confirmed using two analytic models, including the Coulomb potential and energy. We then implement the full-potential RSM using the Green's function Korringa-Kohn-Rostoker (KKR) method for real applications and compare the results with other first-principle methods and experimental data, showing that they are equally as accurate.

DOI: 10.1103/PhysRevB.106.235114

I. INTRODUCTION

All-electron Korringa [1] and Kohn and Rostoker [2] (KKR) electronic structure methods based on multiple-scattering theory are powerful and computationally efficient methods, especially when reformulated as a Green's function [3,4] (GF-KKR), for treating periodic solids or complex condensed-matter systems with point defects [5] and chemical and magnetic disorder in alloys [6–10] and associated transport [11,12] and, recently, for simulating a superconducting state via the Kohn–Sham–Bogoliubov–de Gennes equation [13–16]. Many implementations of (site-centered, all-electron) full-potential (FP) KKR [17–27] employ multipole expansions for solving Poisson equation and shape functions for cellular integrals (both use large, double-internal angular momentum L sums) that can be demanding computationally and exhibit slow convergence, where multipoles are conditionally convergent [18,28] and shape functions [19] exhibit Gibbs phenomena [29–31].

To overcome such issues, the *removed-sphere method* (RSM) [32] is employed, which requires single-L sums to solve Poisson equation (no multipoles), and we reformulate the RSM with full Ewald expressions to calculate reliably any structural configuration or symmetry-breaking cases, such as atomic displacements off ideal positions needed for elastic constant calculations. Alam *et al.* [33] extended the RSM to avoid multipoles and replaced shape functions with isoparametric integration [28]. However, this version lacked the Ewald formulation and so suffered from inaccurate real-space summations, save for symmetric bulk cases.

This full-potential RSM with Ewald expressions for solving Poisson equation should benefit many applications. In particular, GF-KKR is a powerful method for addressing systems with chemical or magnetic disorder and point defects (e.g., vacancies and antisites). This is achieved by combining GF-KKR with the coherent-potential approximation [6,7,34–36] or dynamical cluster approximation [37] for real systems [38,39] that treats the effects of disorder on equal footing with electronic structure, which cannot be treated directly using traditional band theory. GF-KKR succeeds mainly because it separates the single-site scattering matrix $t_L(\epsilon)$ in a site-dependent spherical-harmonic $Y_L(\hat{\mathbf{r}})$ basis set from the underlying structure constants $G_0(\epsilon;\mathbf{k})$, depending on complex energy ϵ and the reciprocal-space vector $\mathbf{k}$. Notably, when formulated properly, including GF-based FP-KKR-RSM, scattering properties can be evaluated in parallel over basis sites, energies, and k points for computational efficiency and near-linear scaling in basis sites [40,41].

Here, we derive the generalized RSM via a full Ewald formulation that accurately solves the Poisson equation. Two analytic bulk electronic models are tested for convergence properties using a single-L sum, showing an error of 10^{-6} for $L_{\max} = 8$. We then implement the RSM in a GF-KKR code and compare FP-KKR-RSM results with those from standard FP methods and experiments. While KKR was originally formulated exactly for close-packed-crystalline metals using potentials from muffin-tin (MT) approximations [1,2,42] or atomic sphere approximations (ASAs) [43], FP-KKR-RSM works for convex Voronoi polyhedra (VPs) in systems with reduced symmetry, like open structures, where nonspherical contributions are non-negligible.

*ning@ameslab.gov
†ddj@ameslab.gov

With a one-to-one mapping between charge density and the potential [44], the density $\rho(\mathbf{r})$ is given by the Green's function $G(\epsilon;\mathbf{r})$, and the KKR-RSM Coulomb potential $V(\mathbf{r})$ is given by Poisson equation [here, in atomic units (Ry) $e^2 = 2$], where $\rho^{\text{total}}(\mathbf{r}) = \rho(\mathbf{r}) - \sum_R Z^R \delta(\mathbf{r} - \mathbf{R})$ with atomic number Z,

$$4\pi e^2 \rho^{\text{total}}(\mathbf{r}) = -\nabla^2 V(\mathbf{r}). \tag{1}$$

With distinct neighbors at $\mathbf{R}$, the solution at the central site ($\mathbf{R} = 0$), denoted by a superscript 0, is

$$V(\mathbf{r}) = 2\sum_R \left[\int_{\Omega_R} \frac{\rho^R(\mathbf{r}')d\mathbf{r}'}{|\mathbf{r} - (\mathbf{r}' + \mathbf{R})|} - \frac{Z^R}{|\mathbf{r} - \mathbf{R}|}\right]$$
$$= V^{\text{intra}}(\mathbf{r}) + V^{\text{inter}}(\mathbf{r}), \tag{2a}$$
$$V^{\text{intra}}(\mathbf{r}) = \left[\int_{\Omega_0} d\mathbf{r}' \frac{2\rho^0(\mathbf{r}')}{|\mathbf{r} - \mathbf{r}'|} - \frac{2Z^0}{r}\right], \tag{2b}$$
$$V^{\text{inter}}(\mathbf{r}) = \sum_{\mathbf{R}\neq 0}\left[\int_{\Omega_R} \frac{d\mathbf{r}' 2\rho^R(\mathbf{r}')}{|\mathbf{r} - (\mathbf{r}' + \mathbf{R})|} - \frac{2Z^R}{|\mathbf{r} - \mathbf{R}|}\right]. \tag{2c}$$

Equation (2) is easily solved for MT/ASA potentials and charge densities [42]. However, a full-potential/density solution is demanding and complicated owing to the dependence on VP shape and its neighbors. For a VP, $V^{\text{intra}}(\mathbf{r})$ is easily obtained by expanding the propagator $|\mathbf{r} - \mathbf{r}'|^{-1}$ in terms of Y_L (Sec. II). However, methods differ on how to handle intercell $V^{\text{inter}}(\mathbf{r})$ terms. van W Morgan [45] expanded the propagator $|\mathbf{r} - \mathbf{r}' - \mathbf{R}|^{-1}$ in a VP circumscribing sphere and used shape functions to get the contributions by multipoles; Weinert [46] used multipole potentials based on a Dirichlet problem for a sphere within the full-potential linearized augmented plane wave method (FLAPW) using local Y_L and plane waves. In cellular methods, expansion of the propagator involving nearest neighbors causes ill convergence, requiring larger internal double-L sums [19,33]. Gonis *et al.* [47] and Vitos and Kollár [48] shifted the propagator by a constant vector $\mathbf{b}$ (and then shifted it back) to partially address this problem, but convergence requires large double-L sums, and convergence is slower with increasing L. Schadler [18] expanded the propagator into four different geometrical $(r_<, r_>)$ cases to remove restrictions on the VP shape, requiring multipoles and corrections for space-filling charge densities. Using Green's theorem, Zhang *et al.* [49] changed the volume integral to surface integrals, requiring facet-dependent wave-function calculations for each VP, which are slower depending on how many VP shapes and inequivalent sites are needed. All the above methods have convergence issues due to multipoles in Y_L expansions. As already noted, Alam *et al.* [33] eliminated multipoles in the RSM [32] and replaced shape functions with isoparametric integration [28], but their formulation used limited real-space neighbor sums and so is not generally applicable.

Here, we generalize the FP-KKR-RSM to solve the Poisson equation in a charge-neutral system using a full Ewald formulation for accuracy and to eliminate convergence problems caused by symmetry breaking. In Sec. II, we present a generalized RSM formulation and properties, and in Sec. III, we address numerical accuracies. The Appendixes provide detailed derivations of equations and properties. Then, in Sec. IV the RSM efficiency and accuracy are verified and compared to two analytic models, i.e., a "jellium" model [50] with an array of nuclear charges Z compensated by a homogeneous electron gas and a charge-density model [45] with $Z = 0$. Section V provides an implementation of the GF-KKR-RSM applied to elemental metals and compounds, with comparison to results from standard FP methods. Section VI summarizes our work.

II. THEORETICAL METHODS

For a given periodic charge density (CD) defined for convex, space-filling VPs, charge balanced by a lattice of positive nuclear charges Z, the Coulomb potential, following Alam *et al.* [33] and Nicholson and Shelton [32], can be accurately determined by coefficients found within the VP where the circumscribing spheres of the nearest neighbors do not overlap, giving a simple result:

$$V(\mathbf{r}) = \sum_L \left[V_L^{\text{intra}}(r) + \alpha_L r^l\right] Y_L(\mathbf{r}), \tag{3}$$

with

$$V_L^{\text{intra}}(r) = \int_0^{r_{\text{CS}}} d\mathbf{r}' \frac{8\pi\rho^{ex}(\mathbf{r}')}{2l+1} \frac{r_<^l}{r_>^{l+1}} Y_L^*(\mathbf{r}') - \frac{2Z}{r}, \tag{4}$$

where $r_< = \min\{r, r'\}$, $r_> = \max\{r, r'\}$, and $L = (l, m)$ labels the expansion of a spherical-harmonic basis $\{Y_L\}$. The extended charge density (ECD) $\rho^{ex}(\mathbf{r})$ is defined up to the circumscribing sphere (with a radius r_{CS}) of the central VP. The expansion coefficients α_L of the Hartree potential is composed of two contributions: one is a_L due to all neighbors, defined by

$$a_L = \frac{8\pi}{2l+1}\sum_{\mathbf{R}\neq 0}\left(\int_{\Omega_R} d\mathbf{r}' \overline{\rho}^{\mathbf{R}}(\mathbf{r}') \frac{Y_L^*(\widehat{\mathbf{r}' + \mathbf{R}})}{|\mathbf{r}' + \mathbf{R}|^{l+1}} - Z^{\mathbf{R}} \frac{Y_L^*(\widehat{\mathbf{R}})}{|\mathbf{R}|^{l+1}}\right), \tag{5}$$

where $\overline{\rho}^{\mathbf{R}}(\mathbf{r})$ is the truncated charge density (TCD) defined in the VP, denoted by Ω_R, located at $\mathbf{R}$; the other is the near-field correction (NFC) in the "moon" region between the VP surface $S(\Omega)$ and the CS, defined by

$$\alpha_L^{\text{NFC}} = -\frac{8\pi}{2l+1}\int_{S(\Omega)}^{r_{\text{CS}}} d\mathbf{r}' \rho^{ex}(\mathbf{r}') \frac{Y_L^*(\widehat{\mathbf{r}'})}{|\mathbf{r}'|^{l+1}}. \tag{6}$$

Alam *et al.* [33] calculated a_L using the charge density over the integral inside a VP utilizing isoparametric integration and then summed the integrals at different $\mathbf{R}$ up to the eighth shell. Accurate results for α_L were obtained, except for α_0 (which depends on $1/|R|$ summed over the lattice, so the direct sum is slowly and nonuniformly convergent; see their Table I); hence, it requires an Ewald method. Their method works well for, e.g., ideal-bulk materials but not for materials with lower symmetry, like cubic systems with atom displacements, such as those needed for elastic constant calculations. These errors arise when symmetry breaking happens as some $\mathbf{R}$ shells are broken into two (or more) subshells that have similar but opposing contributions and should have cancellations. Thus, sums may have different and nonconvergent results with the choice of different shell cutoffs.

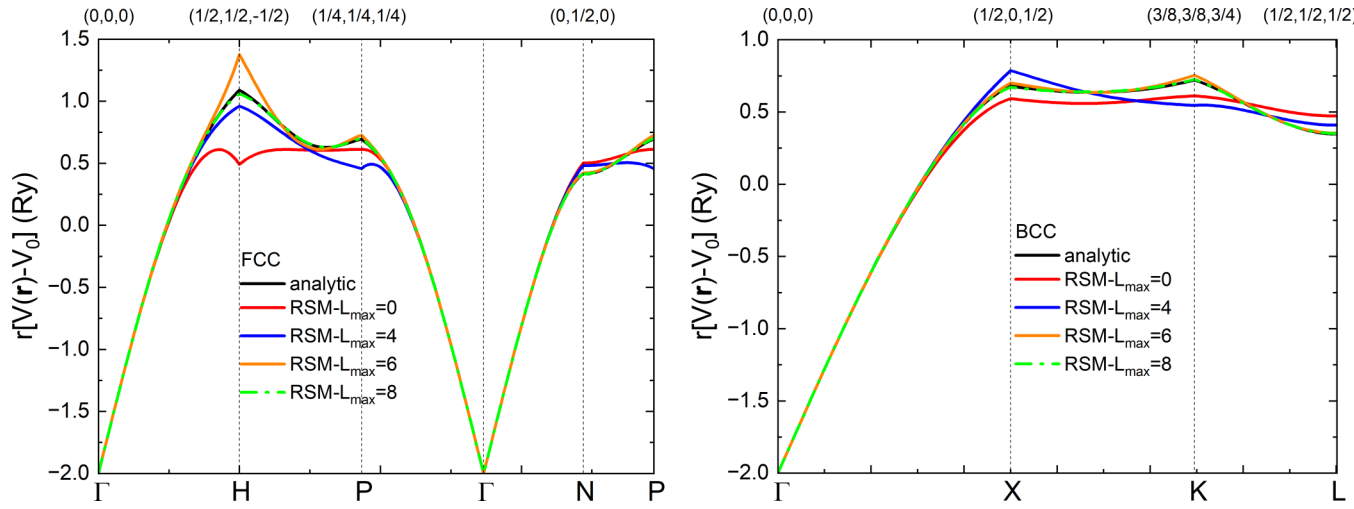

FIG. 1. Convergence of the RSM potential vs $L_{\max}$ for the jellium model along high-symmetry paths in fcc (left) and bcc (right) Wigner-Seitz cells. At $L_{\max} = 8$, the RSM potential and analytic result agree as in Table I. In fractional coordinates, $\Gamma = (0, 0, 0)$, $H = (0.5, 0.5, -0.5)$, $P = (0.25, 0.25, 0.25)$, $N = (0, 0.5, 0)$, $X = (0.5, 0, 0.5)$, $K = (0.375, 0.375, 0.75)$, and $L = (0.5, 0.5, 0.5)$.

As such, we employed Ewald methods to give practical and accurate expressions to calculate a_L, namely,

$$a_L = \frac{8\pi}{2l+1}\left[\int_\Omega d\mathbf{r}'\rho(\mathbf{r}')A_L(\mathbf{r}') - ZA_L(0)\right], \tag{7}$$

where

$$A_L(\mathbf{r}') = A_L^{(S)}(\mathbf{r}') + A_L^{(L)}(\mathbf{r}') + A_L^{(0)}(\mathbf{r}'). \tag{8}$$

In real space, the contributions are short-range $A_L^{(S)}$, long-range $A_L^{(L)}$ (so short range in reciprocal space), and self-interaction $A_L^{(0)}$, which can be written as

$$A_L^{(S)}(\mathbf{r}') = \sum_{\mathbf{R}\neq 0} \frac{Y_L^*(\widehat{\mathbf{r}'+\mathbf{R}})}{|\mathbf{r}'+\mathbf{R}|^{l+1}} Q\left(l+\frac{1}{2}, \sigma^2 T^2\right), \tag{9}$$

$$A_L^{(L)}(\mathbf{r}') = \frac{4\pi}{\Omega}\sum_{\mathbf{K}\neq 0} \frac{e^{\left(\frac{-K^2}{4\sigma^2}\right)}}{K^{2-l}} \frac{i^l Y_L^*(\widehat{\mathbf{K}})}{(2l-1)!!} - \delta_{L,00}\frac{\sqrt{\pi}}{2\Omega\sigma^2}, \tag{10}$$

$$A_L^{(0)}(\mathbf{r}') = -\frac{Y_L^*(\widehat{\mathbf{r}'})}{|\mathbf{r}'|^{l+1}} P\left(l+\frac{1}{2}, \sigma^2|\mathbf{r}'|^2\right) \text{ for } R = 0, \tag{11}$$

where σ is the Ewald parameter, Ω is the unit cell volume, and $\mathbf{K}$ is the reciprocal lattice vectors. $Q(s, x)$ is the incomplete gamma function [51], defined as a ratio, as provided by the algorithm in, e.g., *Numerical Recipes in C* [52]

$$Q(s,x) \equiv \frac{\Gamma(s,x)}{\Gamma(s)} \equiv \frac{1}{\Gamma(s)}\int_x^\infty dt\, e^{-t}t^{s-1}, \tag{12}$$

which can be used to obtain numerically accurately the RSM short-range $A_L^{(S)}$ and $P(s, x) = 1 - Q(s, x)$. See Appendix A for a detailed derivation.

In summary, the solution to the Poisson equation (3) is coefficients $\alpha_L = a_L + \alpha_L^{\text{NFC}}$ with α_L^{NFC} from Eq. (6). The coefficients a_L are obtained from Eqs. (7)–(11). One no longer needs to worry about internal L-convergence issues from multipoles and VP shapes found in other methods. $A_L(\mathbf{r}')$ is a structure-dependent quantity that can be calculated once and saved for the whole self-consistent-field iteration if *ab initio* molecular dynamics is not being carried out. The Ewald parameter is chosen by an optimization method [53].

III. IMPLEMENTATION

Here, we would like to denote two charge densities: a TCD $\overline{\rho}(\mathbf{r})$, ending at the VP surface, and the ECD $\rho^{ex}(\mathbf{r})$, continued to the CS beyond the VP. For solids with space-filling VPs, the CD is defined inside the VP in terms of wave functions or Green's functions. The CD in this region is identical to the TCD. The relationship between TCD and ECD is (see Fig. 1 in Ref. [33])

$$\overline{\rho}(\mathbf{r}) = \rho^{ex}(\mathbf{r})\theta(\mathbf{r}), \tag{13}$$

where $\theta(\mathbf{r})$ is the shape function of the VP, given by

$$\theta(\mathbf{r}) = \begin{cases} 1 & \text{for } \mathbf{r} \in \text{VP}, \\ 0 & \text{for } \mathbf{r} \notin \text{VP}. \end{cases} \tag{14}$$

One can see that ECD is just the regular definition of CD in an adjusted domain and TCD is the same as ECD for every point in the space of a VP.

The symmetry properties of a periodic symmetric charge distribution $\rho^{\mathbf{R}}(\mathbf{r})$ require that $\rho^{\mathbf{R}}(\mathbf{r}') = \rho^0(\mathbf{r}')$ if $\mathbf{R}$ is a primitive translation vector. Then, due to the symmetry of complex spherical harmonics, α_L satisfies

$$\alpha_{l,-m} = (-1)^m \alpha_{l,m}^*. \tag{15}$$

TABLE I. Accuracy check of Coulomb energy U for the jellium model in both bcc and fcc structures. U^{RSM} are results calculated using Eq. (19) with $l_{\max} = 8$. U^{exact} are exact results calculated using Eq. (18). Both are multiplied by a factor of r_{ASA}/Z^2 to get familiar literature values.

Structure	U^{RSM}	U^{exact}	$U^{\text{RSM}} - U^{\text{exact}}$
fcc	1.791745042	1.791747222	-2.180×10^{-6}
bcc	1.791859712	1.791858445	1.267×10^{-6}

In addition, if the crystal has an inversion point, a_L with odd l must vanish, and these symmetry relations hold also for the NFC terms. Thus, by the symmetry property (15), only the upper half needs to be calculate, while the remainder is obtained by symmetry (see Appendix B for a proof).

We note that the range of integration in Eq. (8) from Ref. [33] should include only the moon region between the VP and the CS (not just over the VP). This is reflected in our updated Eq. (6), which can be derived from Eq. (7) in that paper [33] (this equation is missing a spherical harmonic), leading to

$$\sum_L \frac{8\pi}{2l+1}\left[\omega_L(r) + r^l \int_r^{r_{\rm CS}} d\mathbf{r}' \frac{\overline{\rho}(\mathbf{r}')Y_L^*(\widehat{\mathbf{r}'})}{(r')^{l+1}}\right]. \quad (16)$$

IV. REMOVED-SPHERE METHOD SOLUTION FOR EXACT MODELS

The RSM with an Ewald sum is tested for two analytic models to address accuracy and its convergence in L.

A. Madelung's jellium model

The jellium model is very close to the situation in a simple alkali metal; that is, it has a lattice of positive nuclear charges Z surrounded by a constant negative electronic charge density that ensures charge neutrality. Slater derived an analytic solution to its potential [50], i.e.,

$$V(\mathbf{r}) = 2Z\left[\sum_{\mathbf{R}} \frac{1}{|\mathbf{r}-\mathbf{R}|}\mathrm{erfc}(\sigma|\mathbf{r}-\mathbf{R}|) + \frac{4\pi}{\Omega}\sum_{\mathbf{K}\neq 0}\frac{\exp\left(\frac{-K^2}{4\sigma^2}\right)}{K^2}e^{i\mathbf{K}\cdot\mathbf{r}} - \frac{\pi}{\Omega\sigma^2}\right] + V_0. \quad (17)$$

Here, σ is the optimized Ewald parameter. Note that Eq. (17) does not depend on σ because its first derivative with respect to σ is zero. Ω is the volume of the unit cell, and V_0 is an arbitrary constant. Note that $V(\mathbf{r})$ has a singularity at $r = 0$ for $R = 0$. The Coulomb energy for one unit cell with a lattice constant a has an analytic form:

$$U = \left(\frac{Z^2}{r_{\rm ASA}}\right)\frac{r_{\rm ASA}}{a}\left[\sum_{\mathbf{R}\neq 0}\frac{\mathrm{erfc}(\sigma|\mathbf{R}|)}{|\mathbf{R}|} + \frac{4\pi}{\Omega}\sum_{\mathbf{K}\neq 0}\frac{\exp\left(\frac{-K^2}{4\sigma^2}\right)}{K^2} - \frac{\pi}{\Omega\sigma^2} - \frac{2\sigma}{\sqrt{\pi}}\right]. \quad (18)$$

We now show that the RSM results found numerically are very accurate compared to the analytic results for the jellium model given in Eqs. (17) and (18). For simplicity, we choose $Z = 1$ and $a = 1$. The potential denoted by $V^{\rm RSM}(\mathbf{r})$ is obtained from Eqs. (3), (4), and (7)–(11). According to the definition of the total Coulomb energy in a solid, one can derive a simple form of the Coulomb energy in a unit cell given by

$$U^{\rm RSM} = \frac{1}{2}\left[\int_\Omega d\mathbf{r}\rho(\mathbf{r})V^{\rm RSM}(\mathbf{r}) - ZV^M(0)\right], \quad (19)$$

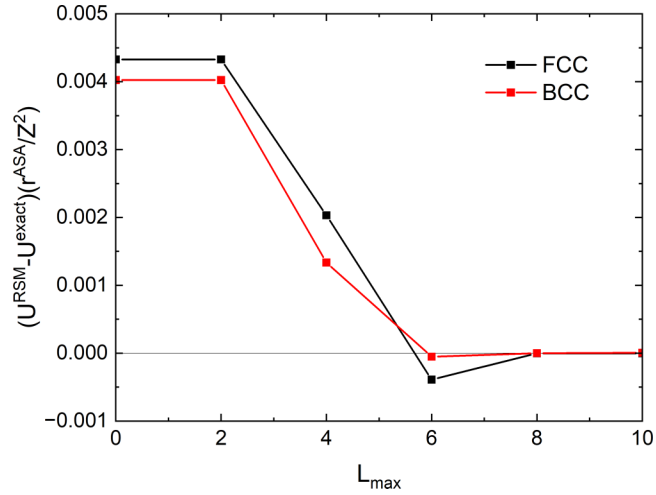

FIG. 2. For jellium in both fcc and bcc structures, we plot the RSM Coulomb energy error (relative to exact values given in Table I) vs $L_{\rm max}$ used in the potentials to show the general expected convergence. For only $L = 0$ the atomic-sphere approximation value is 1.8 for fcc and bcc, with an error of about 0.008 in the given units.

where V^M is the generalized Madelung potential that is the Coulomb potential without the term $2Z/r$. As no direct evaluation of V^M at $r = 0$ is forthcoming, an indirect result from the Dirichlet boundary-value problem for a sphere with radius S is given by [46]

$$V^M(0) = V_{00}^{\rm RSM}(S)Y_{00}(\hat{S}) + \frac{2(Z-Q)}{S} + 2\sqrt{4\pi}\int_0^S dr\, r\rho_{00}(r), \quad (20)$$

where Q is the charge in the sphere. Equation (20) is independent of the radius S. For a charge-neutral system, Eq. (19) is invariant for any constant shift of the Coulomb potential as a shift exists in both $V^{\rm RSM}(\mathbf{r})$ and $V^M(0)$.

In Fig. 1, we compare the analytic potential and numerical RSM potential for $l_{\rm max} = 0, 4, 6, 8$. $V^{\rm RSM}(\mathbf{r})$ has good convergence in $l_{\rm max}$, which is also true for the accuracy. Table I lists the Coulomb energies that have an accuracy of six decimal places when $V^{\rm RSM}(\mathbf{r})$ is calculated up to $l_{\rm max} = 8$. So even if $V^{\rm RSM}$ for $l_{\rm max} = 8$ has low accuracy in areas at some high-symmetry (real-space) points, variational accuracy of the energy is still reached.

To show the L convergence of the RSM Coulomb energy (19), we plot in Fig. 2 the values of $U^{\rm RSM} - U^{\rm exact}$ versus $L_{\rm max}$ truncation of the potentials. Clearly, the Coulomb energy error is 10^{-6} when $L_{\rm max} = 8$ (see Table I) and lower when $L_{\rm max} = 10$. A similar behavior was shown in KKR-RSM self-consistent calculations (without Ewald sums [33]) in ideal bcc and fcc lattices.

B. van W Morgan electronic density model

The van W Morgan density is a pure and virtual electronic system; that is, the conventional nuclear charge $Z = 0$ [45].

TABLE II. For a van W Morgan density in the fcc structure, an accuracy check of the RSM coefficients α_L. $\alpha_L^{\rm RSM}$ are calculated from Eq. (7). $\alpha_L^{\rm exact}$ are exact results from Eq. (23).

l	m	$\alpha_L^{\rm RSM}$	$\alpha_L^{\rm exact}$	$\alpha_L^{\rm RSM}-\alpha_L^{\rm exact}$
0	0	2.004394847	2.004395351	-5.04×10^{-7}
4	0	−6.750338053	−6.750337763	-2.90×10^{-7}
4	4	−4.034098760	−4.034098340	-4.20×10^{-7}
6	0	−8.529402076	−8.529486772	8.4696×10^{-5}
6	4	15.957208937	15.957208475	4.62×10^{-7}
8	0	4.330420886	4.330470875	-4.9989×10^{-5}
8	4	1.628407854	1.628476693	-6.8839×10^{-5}
8	8	2.481167049	2.481185360	-1.8311×10^{-5}

Its charge density is constructed by plane waves given by

$$\rho(\mathbf{r}) = B\sum_n e^{i\mathbf{T}_n\cdot\mathbf{r}}, \tag{21}$$

where $\{\mathbf{T}_n\}$ is a set of the shortest translation vectors in the reciprocal space and B is an arbitrary amplitude, chosen to be 0.5 here. If a fcc structure is considered, the vector set $\{\mathbf{T}_n\}$ has a total of eight vectors along the [1,1,1] direction. A bcc structure has a total of 12 $\mathbf{T}_n$ along the [1,1,0] direction. Obviously, $\rho(\mathbf{r})$ is real with a variable sign because of the symmetric $\{\mathbf{T}_n\}$ and plane waves. One can easily verify that charge neutrality is guaranteed by the fact that the charge in the inscribed sphere (IS) is equal to the interstitial region between the IS and VP boundary but opposite in sign. This model gives the analytic Coulomb potential, with $T=|\mathbf{T}_n|$,

$$V(\mathbf{r}) = 8\pi\rho(\mathbf{r})T^{-2} + V_0. \tag{22}$$

By expanding plane waves in charge density and rewriting $V(\mathbf{r})$ in the form of Eq. (3), one obtains analytic RSM coefficients that include NFCs from near neighbors,

$$\alpha_L = \frac{8\pi B}{T(2l+1)r_{BS}^{l-1}}\, j_{l-1}(Tr_{BS})C_L + V_0\sqrt{\pi}\delta_{l,0}, \tag{23}$$

where $C_L = 4\pi i^l\sum_n Y_L(\hat{\mathbf{T}}_n)$, which is real for fcc and bcc structures, and $j_l(r)$ are spherical Bessel functions. The $\alpha_L^{\rm RSM}$ values obtained from Eq. (7) and the analytic $\alpha_L^{\rm exact}$ from Eq. (23) are listed in Tables II (fcc) and III (bcc). Here, we set the arbitrary constant $V_0=0$.

All $\alpha_L^{\rm RSM}$ are calculated with a common optimized Ewald parameter σ and the same VP integral mesh of $14\times14\times14$ points. Up to $l=4$, an accuracy of seven decimal places is obtained. Although accuracy is decreased with increasing l, five-decimal-place accuracy is reached for the rest. One can obtain better accuracy by adjusting the VP integral mesh for $l>4$. However, the bigger l is, the smaller the role $V_L(r)$ plays in the total potential $V(\mathbf{r})$ is. By balancing accuracy and efficiency, one common optimized σ and one common integral mesh are good enough. One can see this in the comparison of $V(\mathbf{r})$ below.

TABLE III. Same as Table II, except for the bcc structure.

l	m	$\alpha_L^{\rm RSM}$	$\alpha_L^{\rm exact}$	$\alpha_L^{\rm RSM}-\alpha_L^{\rm exact}$
0	0	1.707148777	1.707149398	-6.21×10^{-7}
4	0	−3.873255476	−3.873253011	-2.465×10^{-6}
4	4	−2.314713448	−2.314711405	-2.043×10^{-6}
6	0	6.511561618	6.511542304	1.9314×10^{-5}
6	4	−12.182027075	−12.181980180	-4.6895×10^{-5}
8	0	4.286146333	4.286127909	1.8424×10^{-5}
8	4	1.611887235	1.611801471	8.5764×10^{-5}
8	8	2.455671485	2.455778600	-1.07115×10^{-4}

To check convergence in the expansion in Eq. (3), we calculated $V(\mathbf{r})$ for different cutoff $l_{\rm max}$ for the coefficients $\alpha_L^{\rm RSM}$ and compared the values to analytic ones (see Fig. 3). One can see that both fcc and bcc structures show the same convergence behavior in L. $V^{\rm RSM}(\mathbf{r})$ evaluated up to $l_{\rm max}=0$ or 4 deviates significantly from the analytic values. When $l_{\rm max}=6$, much better accuracy is reached, except for the small area around some special high-symmetry (real-space) points, like the H point in fcc structures and X and K points in bcc structures. Alam *et al.* [33] found that the slow convergence in these areas was mainly due to larger NFCs to the potential. Perfect agreement with analytic results was arrived at for $l_{\rm max}=8$ and accuracies of 10^{-8} Ry around the Γ point and 10^{-6} Ry for other areas, except for the slow convergent areas, where it is 10^{-4} Ry. This supports the statements about the Ewald parameter and integral meshes in the previous paragraph.

Using the van W Morgan model, we see that accurate coefficients α_L are obtained using the RSM with good convergence for practical calculations up to $l_{\rm max}=8$, like in FLAPW, and there are no additional internal L sums required. The jellium model shows that the RSM solves Coulomb energy and potential accurately for a real electronic system.

C. Near-field corrections

The "near-field" terms arise from the fact that the condition $r\leqslant|\mathbf{r}'+\mathbf{R}|$ for expanding $1/|\mathbf{r}-(\mathbf{r}'+\mathbf{R})|$ cannot be satisfied in the whole VP (see Fig. 1 in Ref. [33]). Thus, the potential from the summation of the intracell $V^{\rm intra}(\mathbf{r})$ and far-multipole corrections $V^{\rm FMC}(\mathbf{r})=\sum_L a_L r^l Y_L(\mathbf{r})$ cannot correctly express the solution to the Poisson equation. Near-field corrections $V^{\rm NFC}(\mathbf{r})$ from Eq. (6) solve the problem and have perfect agreement with analytic results in Secs. IV A and IV B.

We compare the analytic solution to the numerical RSM solution [Eq. (3)], plotting in Fig. 4 all three contributions and their various sums [intracell potential $V^{\rm intra}(\mathbf{r})$; intercell potential $V^{\rm FMC}(\mathbf{r})$, including far-field Madelung contributions (FMCs); and near-field corrections $V^{\rm NFC}(\mathbf{r})$ arising from the region between the central cell and neighbors that have overlapping circumscribing spheres]. Both $V^{\rm intra}(\mathbf{r})$ and $V^{\rm intra}(\mathbf{r})+V^{\rm FMC}(\mathbf{r})$ deviate from $V^{\rm analytic}(\mathbf{r})$ significantly. The NFC term has remarkable values in the whole VP and cancels the summation $V^{\rm intra}(\mathbf{r})+V^{\rm FMC}(\mathbf{r})$, so that $V^{\rm RSM}(\mathbf{r})$ agrees fantastically with $V^{\rm analytic}(\mathbf{r})$. In addition, NFC is site dependent and thus can be easily implemented in parallel computation. For VPs with elongated or prismlike shapes, one can add empty sites to avoid an abnormality in the NFC. Therefore, our NFC is the key to solving the Poisson equation successfully and avoiding bottlenecks in fast Fourier transform in other electronic structure packages.

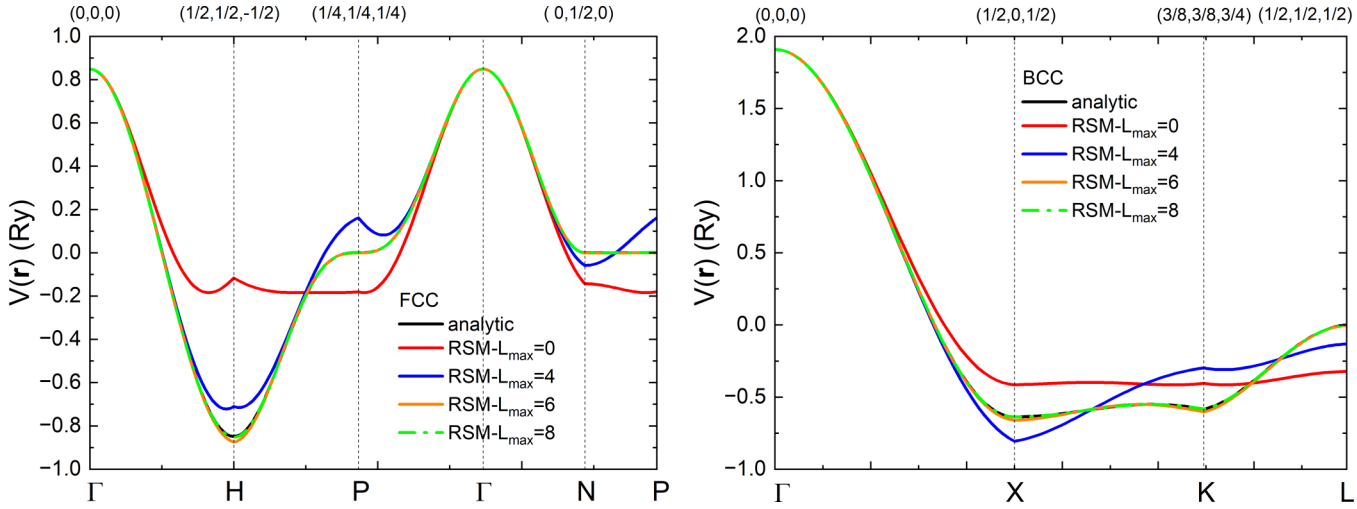

FIG. 3. For the van W Morgan model, convergence $V^{\mathrm{RSM}}(\mathbf{r})$ of $l_{\max}$ on high-symmetry lines of fcc (left) and bcc (right) cells. Fractional coordinates are the same as in Fig. 1.

V. FP-KKR IN THE REMOVED-SPHERE METHOD

What remains is to verify for use in first-principles calculations that a generic RSM numerical solution of the Coulomb potential and energy is possible. An all-electron, Green's function FP-KKR has been implemented within the RSM. With the analytical models tested in the same RSM framework, we apply the methods and compare their accuracy to other electronic structure results, such as FLAPW and a GF-KKR-ASA code using variational energy zeros that compares well with FLAPW for close-packed systems [10,54].

A. Ground-state properties of elemental metals

For FP-KKR-RSM, we find the ground state for elemental metals with a cubic structure, as found by least-squares fit to total energy vs unit cell volume via Murnaghan's equation of state (EOS) [55]. We calculate a total of seven volumes around the ground-state volume for each system. Both the Hedin-Lundqvist parametrization [56] of the local density approximation [57] (LDA) to density functional theory and a gradient-corrected exchange correlation [58] [Perdew-Burke-Ernzerhof (PBE)] are used. For Brillouin zone integration, we used Monkhorst and Pack k meshes [59]. Results for bcc niobium are shown in Fig. 5 along with EOS data (fit error is 1×10^{-8} Ry).

Table IV lists the lattice constants (a, in angstroms) and bulk moduli (B, in gigapascals) for all materials studied in comparison with those obtained from FLAPW [62,64] and VASP [63], as well as with those measured [60,61]. a and B from FP-KKR-RSM for elemental metals agree well with those from other theory results. Notably, LDA is known to overbind relative to PBE, leading to smaller a and thus larger B, whereas PBE [58] adopts a density gradient correction to exchange-correlation potential that leads to increased a and smaller B, in better agreement with experiment. The all-electron FP-KKR-RSM (core levels included) agrees well with room-temperature experimental data, especially B values.

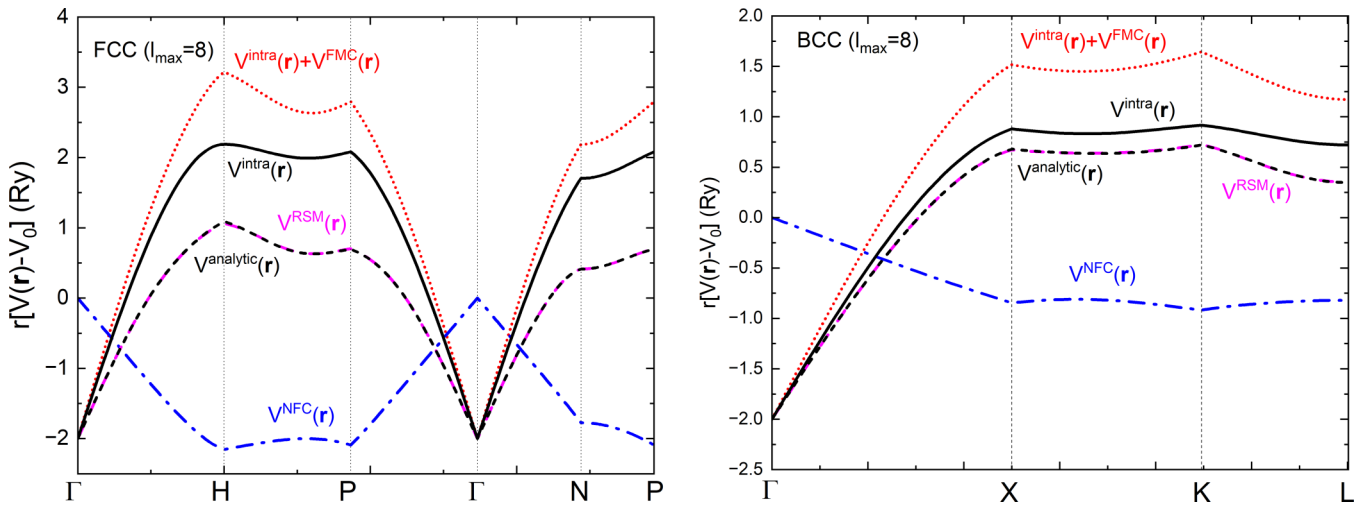

FIG. 4. For jellium, $V^{\mathrm{RSM}}(\mathbf{r})$ ($l_{\max} = 8$) and its components on high-symmetry lines in fcc (left) and bcc (right) cells. Fractional coordinates are the same as in Fig. 1.

TABLE IV. FP-KKR-RSM nonmagnetic results (at 0 K with $L_{max} = 4$ for potential/density) for equilibrium lattice parameters and bulk moduli with a comparison to room temperature measured data [60,61] and to FLAPW [62] in LDA and VASP [63] in PBE.

Element	Structure	a (Å)					B_0 (GPa)				
		LAPW	FP-KKR		VASP	Expt.	LAPW	FP-KKR		VASP	Expt.
		LDA	LDA	PBE	PBE		LDA	LDA	PBE	PBE	
Mo	bcc	3.12	3.11	3.14	3.17	3.15	291	271	262	263	272
Nb	bcc	3.25	3.22	3.29	3.32	3.30	193	172	160	172	170
Ta	bcc	3.24	3.26	3.33	3.32	3.30	224	184	179	193	200
V	bcc	2.93	2.92	2.98	3.00	3.03	196	193	159	181	162
W	bcc	3.14	3.12	3.17	3.19	3.16	333	330	298	298	323
Cu	fcc	3.52	3.52	3.61	3.63	3.61	190	180	149	137	137
Ag	fcc	4.01	3.96	4.10	4.16	4.09	142	151	105	89	101
Au	fcc	4.06	4.01	4.11	4.16	4.08	205	206	148	141	173
Ir	fcc	3.82	3.80	3.85	3.88	3.84	401	406	353	337	355
Ni	fcc	3.42	3.40	3.49	3.52	3.52	261	260	210	194	186
Pd	fcc	3.85	3.82	3.92	3.95	3.89	220	243	178	168	181
Pt	fcc	3.90	3.88	3.95	3.98	3.92	305	327	265	241	278
Rh	fcc	3.76	3.74	3.81	3.84	3.80	309	332	263	254	270

As an accuracy test against one-atom bcc results, we investigate the FP-KKR-RSM total energy as a function of unit cell volume and lattice constant for Nb and Mo with a two-atom bcc cube (denoted B2). The calculated EOS data and Murnaghan's fits are shown in Fig. 5, with both bcc and B2 values listed in Table V. The last column is the deviation of BCC data from B2 data, which show differences of $1–5 \times 10^{-5}$ Ry, showing that the FP-KKR-RSM works in a systematic way.

In short, the GF-based FP-KKR with the RSM potential predicts accurate ground-state structural properties for all materials studied, similar to other methods.

B. Unit cell with atomic displacements

We now address the case where the central atom in a bcc two-atom unit cube (B2-like with a lattice constant of 3.30 Å) is displaced. For Nb, we shift the atom at [0.5,0.5,0.5] (fractional coordinates) along [1,0,0] by $\delta = 0.02$; that is, the new location is at $[0.5 + \delta, 0.5, 0.5]$. We compare in Table VI the coefficients a_L calculated using the real-space sums equation (5) and the Ewald sums equation (7).

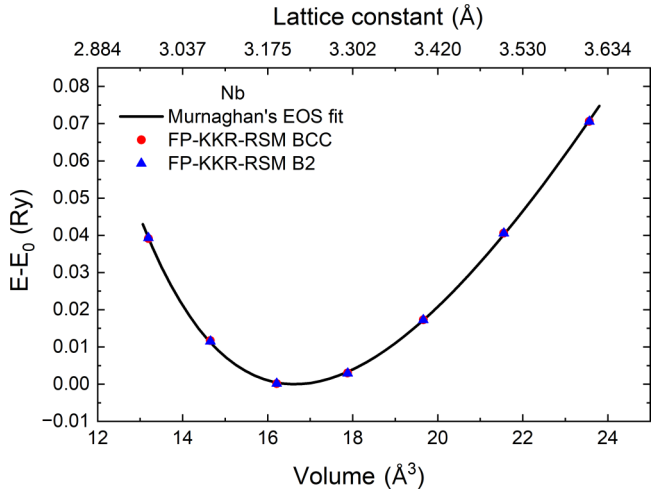

FIG. 5. For one-atom bcc and two-atom bcc (B2) structures, FP-KKR-RSM energy per atom ($L_{max} = 4$ for potential and density) for Nb as a function of the primitive-cell volume (lattice constant), relative to the lowest energy E_0 in Table V.

The first column lists the number neighbors in the shells of an ideal two-atom unit cube for bcc Nb. The second through fifth columns list neighbors and fractional coordinates of shifted shells. The sixth column lists a_{11} summed up to each shell in the shifted system. The last column lists the difference in a_{11} obtained from Eq. (5) and from the exact Ewald expression in Eq. (7). With displacement, we see that **R** shells are broken into subshells. In fact, the result from Eq. (5) is unstable. For example, the first shell [0.5,0.5,0.5] for an ideal two-atom bcc structure with a total of eight neighbors is broken into two subshells located at $[-0.48, 0.5, 0.5]$ and [0.52,0.5,0.5] separately. Similarly, due to symmetry breaking, the fourth and seventh ideal shells are broken into four subshells, where the subshells have close contributions but opposite signs. For instance, the a_{11} contributions of the first two subshells are 1.11800 and −1.11881 Ry/Bohr, which should nearly cancel to give a small value (−0.00081 Ry/Bohr). Clearly, a_{11} from Eq. (5) is wrong and so is inappropriate for cases with symmetry breaking. However, the Ewald-based Eq. (7) is correct, quite stable, and invariant for any Ewald parameter σ. Thus, the RSM provided in this work is more general and necessary for electronic structure calculations.

As a last example, we compute energy versus cell distortion along [100] of a two-atom cube. For Nb with $a_0 =$

TABLE V. Ground-state energies and lattice constants for Nb and Mo calculated with a one-atom bcc or two-atom B2 structure, showing similar errors for both metals.

Element	Parameter	bcc	B2	Difference
Nb	a (Å)	3.21644	3.21613	3.1×10^{-4}
	E_0 (Ry)	−7632.93092	−7632.93097	-5.0×10^{-5}
Mo	a (Å)	3.11289	3.11276	1.3×10^{-4}
	E_0 (Ry)	−8090.91824	−8090.91827	-3.0×10^{-5}

TABLE VI. Real-space and Ewald results for coefficient a_{11} (Ry/Bohr) for a two-atom bcc Nb with the atom at [0.5,0.5,0.5] (fractional coordinates) shifted along [1,0,0] by 0.02. The exact a_{11}^{Ewald} from Eq. (7) is 0.00142 Ry/Bohr. By direct sum, a_{11} from Eq. (5) up to 15 neighbor shells (sixth column) and its error (seventh column), defined as $a_{11}^{\text{real}}/a_{11}^{\text{Ewald}} - 1$, are also shown.

Ideal	Shifted shells				a_{11}^{real}	Error
N	N	l	m	n		
8	4	−0.48	0.5	0.5	1.11800	786.32177
8	4	0.52	0.5	0.5	−0.00081	−1.57259
6	6	1.0	0.0	0.0	−0.00119	−1.84020
12	12	1.0	1.0	0.0	−0.00116	−1.81907
24	4	−1.48	0.5	0.5	0.48703	341.97670
24	8	1.5	−0.48	0.5	0.79717	560.38515
24	8	1.5	0.52	0.5	0.46889	329.20206
24	4	1.52	0.5	0.5	−0.00113	−1.79795
8	8	1.0	1.0	1.0	−0.00111	−1.78386
6	6	2.0	0.0	0.0	−0.00112	−1.79090
24	4	−1.48	1.5	0.5	0.42315	296.99079
24	4	1.5	1.5	-0.48	0.49115	344.87811
24	8	1.5	1.5	0.52	0.41853	293.73727
24	8	1.52	1.5	0.5	−0.00114	−1.80499
24	24	2.0	1.0	1.0	−0.00114	−1.80499

3.30 Å and atoms in the (1,0,0) plane at the origin held fixed, we uniformly stretch a cell along $a[1, 0, 0]$ and monitor the energy of the distorted cell relative to E_0 in Table V. Figure 6 shows two cases (with $a_2 = a_3$), distortion of a_1 with a volume that (1) varies or (2) is fixed at the equilibrium value (which fixes electron density and should be lower in energy as metals in solids like fixed density). Results show the relative accuracy and cost of constraints with distortions. Moreover, fitting the constant-volume data in Fig. 6 via a quadratic form yields an estimate for Young's modulus (i.e., 0.0072 Ry/Bohr^3, or 106 GPa), which is close to the experimental value of 105 GPa.

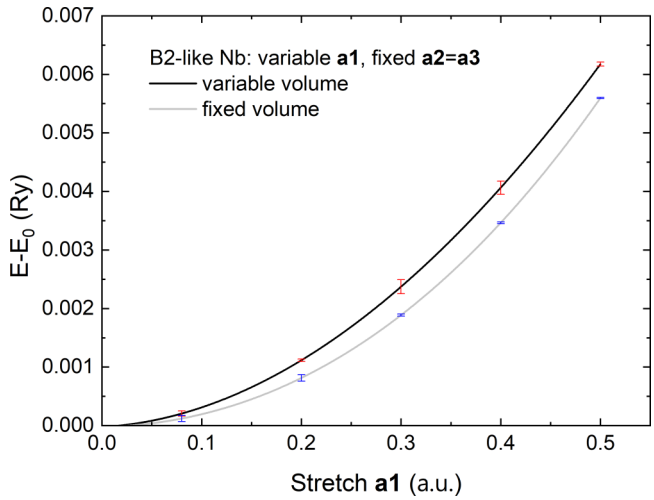

FIG. 6. For B2 Nb in Fig. 5, relative to E_0 in Table V, FP-KKR-RSM energy (Ry) vs the a_1 distortion (a.u.) along [100]. Cube volume $V = a_1a_2a_3$, where $a_i = a$ at E_0. Two distortions with $a_2 = a_3$ were considered, with V variable or fixed (giving fixed electronic density). The accuracy is evident.

VI. CONCLUSION

We presented a practical and accurate numerical solution to the Poisson equation based on the removed-sphere method that avoids various multipole and integration convergence issues for local spherical harmonic basis sets and improves cellular integral convergence (often done with shape functions) with isoparametric integration. To work for general symmetries, a complete Ewald formulation of the RSM was provided and tested using analytic models. The accuracy of the generalized RSM depends on the convergence of coefficients $\alpha_{L=\{l,m\}}$ that give the solution to Poisson equation. We find that they exhibit good convergence for practical calculation at $L_{\max} \leqslant 8$, as also confirmed using analytic models that show the RSM is accurate for both the Coulomb potential and energy.

We also implemented the RSM within a Green's function based FP-KKR, which used charge density expanded in terms of a localized, site-centered basis formed from spherical harmonics, and showed agreement with results from other full-potential/density methods. With symmetry breaking and RSM working, we plan to refine the FP-KKR-RSM symmetry features to improve the speed and convergence for general structures and to extend the method to address forces, such as those needed for atomic relaxations and elastic constant calculations, requiring only convergence in a single-L sum that avoids multipoles.

ACKNOWLEDGMENTS

This work was supported by the U.S. Department of Energy (DOE), Office of Science, Basic Energy Sciences, Materials Science and Engineering Division. Work was performed at Ames Laboratory, which is operated by Iowa State University for the U.S. DOE under Contract No. DE-AC02-07CH11358.

APPENDIX A

Here, a detailed derivation of Eqs. (7)–(11) is presented. Following Alam *et al.* [33], we know that the coefficient a_L is derived by expanding $1/|\mathbf{r} - (\mathbf{r}' + \mathbf{R})|$ based on the condition $r \leqslant |\mathbf{r}' + \mathbf{R}|$. From the Ewald sum,

$$\sum_{\mathbf{R}\neq 0} \frac{1}{|\mathbf{r} - (\mathbf{r}' + \mathbf{R})|} = \phi^{(S)}(\mathbf{r}) + \phi^{(L)}(\mathbf{r}) + \phi^{(0)}(\mathbf{r}), \quad \text{(A1)}$$

where, with $\mathbf{T} \equiv \mathbf{r}' + \mathbf{R}$,

$$\phi^{(S)}(\mathbf{r}) = \sum_{\mathbf{R}\neq 0} \frac{1}{|\mathbf{r} - \mathbf{T}|} \text{erfc}(\sigma|\mathbf{r} - \mathbf{T}|), \quad \text{(A2)}$$

$$\phi^{(L)}(\mathbf{r}) = \frac{4\pi}{\Omega} \sum_{\mathbf{K}\neq 0} \frac{\exp\left(\frac{-K^2}{4\sigma^2}\right)}{K^2} e^{i\mathbf{K}\cdot\mathbf{r}} - \frac{\pi}{\Omega\sigma^2}, \quad \text{(A3)}$$

$$\phi^{(0)}(\mathbf{r}) = -\frac{1}{|\mathbf{r}|} \text{erf}(\sigma|\mathbf{r}|). \quad \text{(A4)}$$

The error function $\mathrm{erf}(x) = (2/\sqrt{\pi})\int_0^x dx e^{-x^2}$, and the complimentary error function $\mathrm{erfc}(x) = 1 - \mathrm{erf}(x)$. If one picks $r \to 0$, it satisfies the condition as well, and then the terms of the Ewald sum, $\phi^{(S)}(\mathbf{r})$, $\phi^{(L)}(\mathbf{r})$, and $\phi^{(0)}(\mathbf{r})$, should be able to be expanded in terms of spherical harmonics as

$$\phi(\mathbf{r}) = \sum_{\mathbf{R}\neq 0} r^l Y_L(\widehat{\mathbf{r}}) A_L, \tag{A5}$$

where A_L are expansion coefficients that do not depend on r and can be defined by

$$A_L = \lim_{r\to 0} \frac{C_l}{r^l} \int d\widehat{\mathbf{r}} \phi(\mathbf{r}) Y_L^*(\widehat{\mathbf{r}}), \tag{A6}$$

where $C_l = 4\pi/(2l+1)$. Let us first derive $A_L^{(S)}$ for $\phi^{(S)}(\mathbf{r})$. We do a variable change $x \equiv |\mathbf{r} - \mathbf{T}|x'$, and then

$$\frac{\mathrm{erfc}(\sigma|\mathbf{r}-\mathbf{T}|)}{|\mathbf{r}-\mathbf{T}|} = \int_\sigma^\infty dx\, e^{-(r^2+T^2)x^2} e^{-i(2ix^2\mathbf{r})\cdot\mathbf{T}}. \tag{A7}$$

We expand the plane wave in the integrand by Bauer's expansion and obtain

$$\begin{aligned} A_L^{(S)} &= \lim_{r\to 0} \frac{C_l}{r^l} \int d\widehat{\mathbf{r}}\, Y_L^*(\widehat{\mathbf{r}}) \sum_{\mathbf{R}\neq 0} \frac{\mathrm{erfc}(\sigma|\mathbf{r}-\mathbf{T}|)}{|\mathbf{r}-\mathbf{T}|} \\ &= \sum_{\mathbf{R}\neq 0} \frac{Y_L^*(\widehat{\mathbf{T}})}{|\mathbf{T}|^{l+1}} \frac{\Gamma\left(l+\frac{1}{2}, \sigma^2|\mathbf{T}|^2\right)}{\Gamma(l+1/2)}, \end{aligned} \tag{A8}$$

where

$$\Gamma(s, \beta^2) = 2\int_\beta^\infty t^{2s-1} e^{-t^2} dt \tag{A9}$$

is the incomplete gamma function with the recursion relation

$$\Gamma(s+1, \beta^2) = s\Gamma(s, \beta^2) + \beta^{2s} e^{-\beta^2}. \tag{A10}$$

The incomplete gamma function [51], as provided by the algorithm in *Numerical Recipes in C* [52], is defined as a ratio, i.e.,

$$Q(s,x) \equiv \frac{\Gamma(s,x)}{\Gamma(s)} \equiv \frac{1}{\Gamma(s)} \int_x^\infty dt\; e^{-t} t^{s-1}, \tag{A11}$$

which is a numerically safe means to determine the short-range contribution $A_L^{(S)}$ in the removed-sphere method, and $P(s,x) = 1 - Q(s,x)$.

Similarly, we expand the plane wave in $\phi^{(L)}(\mathbf{r})$ using Bauer's expansion and obtain

$$\begin{aligned} A_L^{(L)} &= \lim_{r\to 0} \frac{C_l}{r^l} \frac{4\pi}{\Omega} \int d\widehat{\mathbf{r}}\, Y_L^*(\widehat{\mathbf{r}}) \sum_{\mathbf{K}\neq 0} \frac{\exp\left(\frac{-K^2}{4\sigma^2}\right)}{K^2} e^{i\mathbf{K}\cdot\mathbf{r}} - \delta_{L,00}\frac{\sqrt{\pi}}{2\Omega\sigma^2} \\ &= \frac{4\pi}{\Omega} \sum_{\mathbf{K}\neq 0} \frac{e^{\left(\frac{-K^2}{4\sigma^2}\right)}}{K^2} \frac{(iK)^l Y_L^*(\widehat{\mathbf{K}})}{(2l-1)!!} - \delta_{L,00}\frac{\sqrt{\pi}}{2\Omega\sigma^2}. \end{aligned} \tag{A12}$$

The expansion coefficient for $\phi^{(0)}(\mathbf{r})$ is quite simple:

$$A_L^{(0)} = -\frac{Y_L^*(\widehat{\mathbf{r}}')}{|\mathbf{r}'|^{l+1}} P\left(l+\frac{1}{2}, \sigma^2|\mathbf{r}'|^2\right). \tag{A13}$$

Finally,

$$A_L = A_L^{(S)} + A_L^{(L)} + A_L^{(0)}. \tag{A14}$$

APPENDIX B

This Appendix proves the symmetry properties of coefficients α_L. Say we are looking at one point ($\mathbf{r}'$) in a neighbor located at $\mathbf{R}$; there must be a point $\mathbf{r} = -\mathbf{r}'$ in the neighbor located at $-\mathbf{R}$. Therefore, the summation in Eq. (5) will have only terms like

$$\begin{aligned} a_L &= \frac{4\pi}{2l+1}\left[\int_{\Omega_R} d\mathbf{r}' \rho^{\mathbf{R}}(\mathbf{r}') \frac{Y_L^*(\widehat{\mathbf{r}'+\mathbf{R}})}{|\mathbf{r}'+\mathbf{R}|^{l+1}} + \int_{\Omega_{-R}} d\mathbf{r}' \rho^{-\mathbf{R}}(\mathbf{r}') \frac{Y_L^*(\widehat{\mathbf{r}'-\mathbf{R}})}{|\mathbf{r}'-\mathbf{R}|^{l+1}} + \cdots\right] \\ &= \frac{4\pi}{2l+1}\left[\int_{\Omega_R} d\mathbf{r}' \rho^{\mathbf{R}}(\mathbf{r}') \frac{Y_L^*(\widehat{\mathbf{r}'+\mathbf{R}})}{|\mathbf{r}'+\mathbf{R}|^{l+1}} + (-1)^l \int_{\Omega_R} d\mathbf{r}' \rho^{\mathbf{R}}(\mathbf{r}') \frac{Y_L^*(\widehat{\mathbf{r}'+\mathbf{R}})}{|\mathbf{r}'+\mathbf{R}|^{l+1}} + \cdots\right] = 0, \end{aligned} \tag{B1}$$

so if the crystal has inversion symmetry and l is odd, a_L vanishes. The symmetry property of the NFC part can be shown in the same way. The complex spherical harmonics has the symmetry properties,

$$Y_{l,-m} = (-1)^m Y_{l,m}^*. \tag{B2}$$

Thus, the coefficients α_L must satisfy

$$\alpha_{l,-m} = (-1)^m \alpha_{l,m}^*. \tag{B3}$$

[1] J. Korringa, Physica (Amsterdam) **13**, 392 (1947).
[2] W. Kohn and N. Rostoker, Phys. Rev. **94**, 1111 (1954).
[3] T. H. Dupree, Ann. Phys. (NY) **15**, 63 (1961).
[4] F. S. Ham and B. Segall, Phys. Rev. **124**, 1786 (1961).
[5] P. Dederichs, T. Hoshino, B. Drittler, K. Abraham, and R. Zeller, Phys. B (Amsterdam, Neth.) **172**, 203 (1991).
[6] D. D. Johnson, D. M. Nicholson, F. J. Pinski, B. L. Gyorffy, and G. M. Stocks, Phys. Rev. Lett. **56**, 2088 (1986).
[7] D. D. Johnson, D. M. Nicholson, F. J. Pinski, B. L. Gyorffy, and G. M. Stocks, Phys. Rev. B **41**, 9701 (1990).
[8] D. D. Johnson, A. V. Smirnov, J. B. Staunton, F. J. Pinski, and W. A. Shelton, Phys. Rev. B **62**, R11917(R) (2000).

[9] A. V. Smirnov, W. A. Shelton, and D. D. Johnson, Phys. Rev. B **71**, 064408 (2005).
[10] A. Alam and D. D. Johnson, Phys. Rev. B **85**, 144202 (2012).
[11] G. M. Stocks and W. H. Butler, Phys. Rev. Lett. **48**, 55 (1982).
[12] W. H. Butler and G. M. Stocks, Phys. Rev. B **29**, 4217 (1984).
[13] T. G. Saunderson, J. F. Annett, B. Újfalussy, G. Csire, and M. Gradhand, Phys. Rev. B **101**, 064510 (2020).
[14] S. K. Ghosh, G. Csire, P. Whittlesea, J. F. Annett, M. Gradhand, B. Újfalussy, and J. Quintanilla, Phys. Rev. B **101**, 100506(R) (2020).
[15] G. Csire, A. Deák, B. Nyári, H. Ebert, J. F. Annett, and B. Újfalussy, Phys. Rev. B **97**, 024514 (2018).
[16] G. Csire, B. Újfalussy, J. Cserti, and B. Győrffy, Phys. Rev. B **91**, 165142 (2015).
[17] R. Zeller, J. Phys. C **20**, 2347 (1987).
[18] G. H. Schadler, Phys. Rev. B **45**, 11314 (1992).
[19] B. Drittler, M. Weinert, R. Zeller, and P. Dederichs, Solid State Commun. **79**, 31 (1991).
[20] R. K. Nesbet, Phys. Rev. B **45**, 11491 (1992).
[21] W. H. Butler, A. Gonis, and X.-G. Zhang, Phys. Rev. B **45**, 11527 (1992).
[22] X.-G. Zhang, W. H. Butler, D. M. Nicholson, and R. K. Nesbet, Phys. Rev. B **46**, 15031 (1992).
[23] X.-G. Zhang and W. H. Butler, Phys. Rev. B **46**, 7433 (1992).
[24] N. Papanikolaou, R. Zeller, P. H. Dederichs, and N. Stefanou, Phys. Rev. B **55**, 4157 (1997).
[25] T. Huhne, C. Zecha, H. Ebert, P. H. Dederichs, and R. Zeller, Phys. Rev. B **58**, 10236 (1998).
[26] M. Asato, A. Settels, T. Hoshino, T. Asada, S. Blügel, R. Zeller, and P. H. Dederichs, Phys. Rev. B **60**, 5202 (1999).
[27] H. Ebert, J. Braun, D. Ködderitzsch, and S. Mankovsky, Phys. Rev. B **93**, 075145 (2016).
[28] A. Alam, S. N. Khan, B. G. Wilson, and D. D. Johnson, Phys. Rev. B **84**, 045105 (2011).
[29] H. Wilbraham, Cambridge & Dublin Math. **3**, 198 (1848).
[30] J. W. Gibbs, Nature (London) **59**, 200 (1898).
[31] J. W. Gibbs, Nature (London) **59**, 606 (1899).
[32] D. M. C. Nicholson and W. A. Shelton, J. Phys.: Condens. Matter **14**, 5601 (2002).
[33] A. Alam, B. G. Wilson, and D. D. Johnson, Phys. Rev. B **84**, 205106 (2011).
[34] P. Soven, Phys. Rev. **156**, 809 (1967).
[35] B. L. Gyorffy, Phys. Rev. B **1**, 3290 (1970).
[36] G. M. Stocks, R. W. Willams, and J. S. Faulkner, Phys. Rev. B **4**, 4390 (1971).
[37] M. H. Hettler, M. Mukherjee, M. Jarrell, and H. R. Krishnamurthy, Phys. Rev. B **61**, 12739 (2000).
[38] D. A. Biava, S. Ghosh, D. D. Johnson, W. A. Shelton, and A. V. Smirnov, Phys. Rev. B **72**, 113105 (2005).
[39] S. Ghosh, D. A. Biava, W. A. Shelton, and D. D. Johnson, Phys. Rev. B **73**, 085106 (2006).
[40] A. V. Smirnov and D. D. Johnson, Comput. Phys. Commun. **148**, 74 (2002).
[41] A. V. Smirnov and D. D. Johnson, Phys. Rev. B **64**, 235129 (2001).
[42] J. F. Janak, Phys. Rev. B **9**, 3985 (1974).
[43] O. K. Andersen, Phys. Rev. B **12**, 3060 (1975).
[44] P. Hohenberg and W. Kohn, Phys. Rev. **136**, B864 (1964).
[45] J. van W. Morgan, J. Phys. C **10**, 1181 (1977).
[46] M. Weinert, J. Math. Phys. **22**, 2433 (1981).
[47] A. Gonis, E. C. Sowa, and P. A. Sterne, Phys. Rev. Lett. **66**, 2207 (1991).
[48] L. Vitos and J. Kollár, Phys. Rev. B **51**, 4074 (1995).
[49] X.-G. Zhang, W. H. Butler, J. M. MacLaren, and J. van Ek, Phys. Rev. B **49**, 13383 (1994).
[50] J. Slater, *Insulators, Semiconductors and Metals*, International Series in Pure and Applied Physics (McGraw-Hill, New York, 1967).
[51] *Handbook of Mathematical Functions with Formulas, Graphs, and Mathematical Tables*, edited by M. Abramowitz and I. A. Stegun (U.S. Government Printing Office, Washington, DC, 1972).
[52] W. H. Press, S. A. Teukolsky, W. T. Vetterling, and B. P. Flannery, *Numerical Recipes in C*, 2nd ed. (Cambridge University Press, Cambridge, 1992), Sec. 6.2.
[53] R. A. Jackson and C. R. A. Catlow, Mol. Simul. **1**, 207 (1988).
[54] A. Alam and D. D. Johnson, Phys. Rev. B **80**, 125123 (2009).
[55] F. D. Murnaghan, Proc. Natl. Acad. Sci. USA **30**, 244 (1944).
[56] L. Hedin and B. I. Lundqvist, J. Phys. C **4**, 2064 (1971).
[57] W. Kohn and L. J. Sham, Phys. Rev. **140**, A1133 (1965).
[58] J. P. Perdew, K. Burke, and M. Ernzerhof, Phys. Rev. Lett. **77**, 3865 (1996).
[59] H. J. Monkhorst and J. D. Pack, Phys. Rev. B **13**, 5188 (1976).
[60] C. Kittel, *Introduction to Solid State Physics* (John Wiley & Sons, New York, 2005), 8th ed.
[61] H. Schäfer, Ber. Bunsen-Ges. Phys. Chem. **79**, 110 (1975).
[62] M. J. Mehl and D. A. Papaconstantopoulos, Phys. Rev. B **54**, 4519 (1996).
[63] K. Lejaeghere, V. V. Speybroeck, G. V. Oost, and S. Cottenier, Crit. Rev. Solid State Mater. Sci. **39**, 1 (2014).
[64] M. J. Mehl, J. E. Osburn, D. A. Papaconstantopoulos, and B. M. Klein, Phys. Rev. B **41**, 10311 (1990).